Compact Modeling of Spiral Inductors for RF Applications

Ji Chen and Juin J. Liou
Electrical and Computer Engineering Dept.
University of Central Florida, Orlando, FL 32816
Phone: 407-823-5339, Fax: 407-823-5835, E-mail: liou@pegasus.cc.ucf.edu

ABSTRACT

Recent growth in RF applications has increased the use of spiral inductors and thus demanded a more accurate model for such devices. In this paper, we focus on the model development of spiral inductors having symmetrical terminals, but the same approach can be applied readily to asymmetrical inductors. Relevant and important physics such as the current crowding in metal line, frequency-dependent permittivity in oxide, and overlap parasitics are accounted for. Experimental data and results calculated from the existing inductor models are included in support of the model development.

Keywords: spiral inductor, compact model, RF application, nonuniform current distribution

1. INTRODUCTION

Wireless communications is already part of our daily life. To reduce the cost of monolithic microwave integrated circuits (MMICs), passive devices are frequently integrated with active components on the same chip. Spiral inductors are particularly important and widely used in MMICs such as low-noise amplifiers, oscillators, and mixers [1].

Many spiral inductors models have been reported in the literature [2]-[16], and all these models were developed intended for asymmetrical inductors but nonetheless sometimes used for symmetrical inductors. To the best of our knowledge, an accurate and compact symmetrical inductor model is not yet available and urgently needed. Empirical technique based on curve fitting for symmetrical inductors has been reported in [7], but models derived this way cannot be scaled to reflect changes in the inductor's layout or fabrication technology. Commercial electromagnetic field solver may also be used to predict the inductor's performance accurately, but the computation time can be too extensive to be practical.

In this paper, a physics-based model applicable for both symmetrical and asymmetrical inductors will be developed. Model development and the proposed equivalent circuit for symmetrical inductors will first be given in Section 2. In Section 3, results obtained from the present model, existing models, and measurements are compared. Finally, conclusions are given in Section 4.

2. MODEL DEVELOPMENT OF SYMMETRICAL INDUCTOR

Our model development will first focus on symmetrical inductors. In addition, an octagonal spiral pattern will be considered, but the approach applies generally to other non-circular patterns. It has been suggested that the octagonal spiral provides a higher Q factor and lower series resistance than the square pattern [1] and is more area efficient and easier realized than the circular spiral [4]. The consideration of the octagonal in fact makes the model more comprehensive than most existing models which consider only square or hexagonal patterns.

Fig. 1(a) shows a symmetrical, octagon spiral inductor with 3 turns. For such an inductor, the metal track can be divided into 5 segments and 2 overlaps (see Fig. 2(a)), and the improved equivalent circuit for the inductor is given in Fig. 1(b). In Fig. 1(b), each segment box is represented by a lumped model shown in Fig. 1(c). In addition, coupling capacitances between the metal lines and parasitics associated with the overlaps need to be considered. These are accounted for with all the other components besides the segment boxes in Fig. 1(b), where $C_{C,ij}$ is the coupling capacitance between two particular metal lines i and j, C_{mm} represents the capacitance associated with the overlap, C_{ox_up} and C_{sub_up} model the capacitances associated with the oxide and substrate of the underpass metal, respectively, and G_{sub_up} models the substrate conductance of the underpass metal. Note that there are two sets of the overlap parasitic components, and the subscripts 1 and 2 denote the components pertinent to overlaps 1 and 2, respectively. It is worth mentioning that the lumped equivalent circuit in Fig. 1(c) is the sole framework used in the conventional modeling of spiral inductors.

2.1 Nonuniform Current Distribution in Metal Lines

A difficult issue in modeling the spiral inductor is the fact that the current distribution in a metal line is not uniform and is a strong function of its location and operating frequency. Such a nonuniform current distribution is an important

mechanism affecting the inductor performance. Traditionally, the current density in a metal line is considered to be governed by the skin and proximity effects [7-9]. It is more realistic, however, to consider the subject metal line lies in midst of electromagnetic field generated by all the other metal lines. According to the partial-element-equivalent-circuit (PEEC) simulation [10] and 3-D electromagnetic simulation [11], the current distribution in a metal line in general exhibits

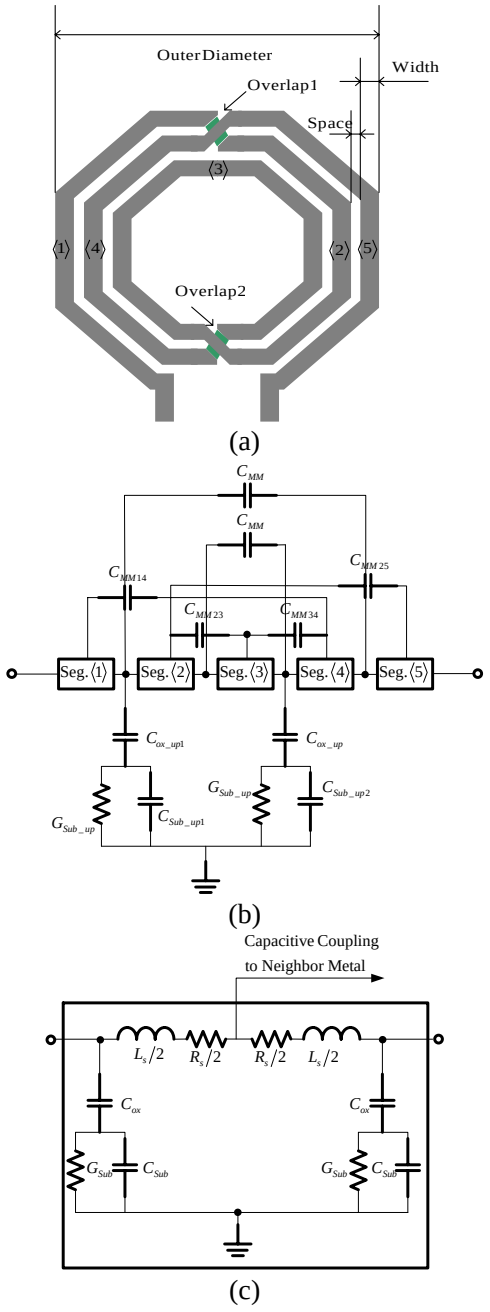

Fig. 1: (a) Schematic of an octagon symmetrical inductor of 3 turns, (b) overall equivalent circuit for the inductor including the segment, capacitive coupling, and overlap components, and (c) equivalent circuit for the segment box in (b).

an exponential decay from the inner edge (side of metal line closer to the center of spiral) to the outer edge (side of metal line farther away from the center of spiral). Furthermore, this exponential-decay distribution is more prominent in the inner turns as the frequency is increased. Fig. 2 shows the current density distributions in segments 1, 4, and 3 (circled in Fig. 2) simulated from an EM simulator. The frequency and location dependencies of the current distribution in the metal lines are clearly illustrated.

We now introduce the concept of the effective line width W_{eff} in which the majority of the current density exists (the region where the first exponent of current density exists). Once W_{eff} is in place, then the nonuniform current distribution effect can be accounted for by replacing all the physical line widths in the model parameters with W_{eff}. The following expressions are proposed to describe the effective line width as a function of the frequency and the segment number (i.e., location of the metal line):

$$w_{eff} = W_{0,i}\left(1-\exp\left(-\frac{w}{W_{0,i}}\right)\right) \quad (1a)$$

$$W_{0,i} = c1\cdot c2^{i-1}\sqrt{\frac{1}{f}} \quad (1b)$$

where w is the physical width of metal line, f is frequency in Hz, i is turn index (i.e., for segments 1 and 5, i=1; segments 2 and 4, i=2; segments 3, i=3), and $c1$ and $c2$ are fitting parameters.

Fig. 3 shows the normalized current distributions in segments 3, 2, and 5 obtained from an EM simulator and the effective line width model. The model results were calculated by first integrating the current distribution simulated from the EM simulator over the physical line width, normalizing it with the current integrated over the effective line width, and then using it as the peak value followed by an exponential decay function. The good agreement demonstrates the soundness of using the effective line width for modeling the frequency- and location-dependent natures of the spiral inductors.

2.2 Modeling the Segment Box

As shown in Fig. 1(c), the model components in the segment box include the series inductance L_S, series resistance R_S, and substrate parasitics.

The metal track in each segment can be further divided into several straight metal lines (for example, 5 straight metal lines for segment 4, see Fig. 1(a)), so that the inductance L_{S_lines} of each straight metal line can be expressed as the self inductance L_{line_self} plus the mutual inductance M from all other metal lines [12]:

$$L_{S\_line} = L_{line\_self} + \sum M \qquad (2)$$

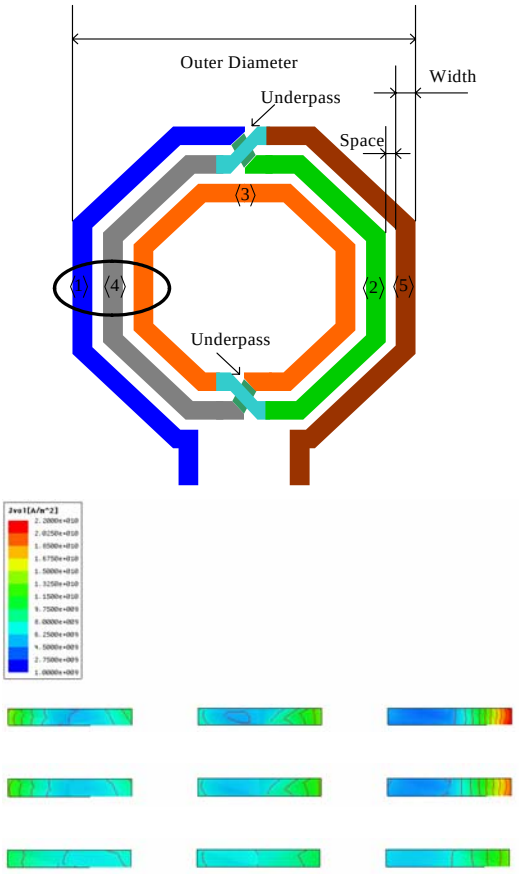

Fig. 2: Current density contours in the three metal lines at three different frequencies simulated from an EM simulator.

As the current redistribute in the metal line at high frequencies, the corresponding inductance and resistance become frequency-dependent. The self-inductance and mutual inductance in (2) were calculated using the method in [13], but with the metal width replaced with the effective line width stated above.

Substrate parasitics result from the electrical coupling between the metal track and substrate, as the metal track of a spiral inductor can be considered as a microstrip on substrate with waves passing through it [13]. Three elements, C_{ox}, G_{sub}, and C_{sub}, are used to model the substrate parasitics (see Fig. 1(c)).

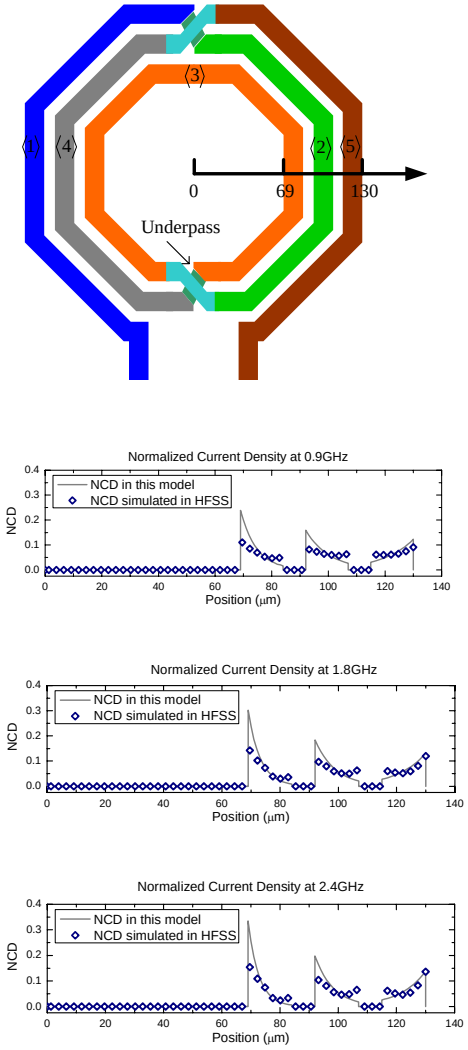

Fig. 3: Comparison of current density distributions in the three metal lines calculated from the present model (lines) and obtained from EM simulations (symbols).

2.3 Modeling Components Outside Segment Box

In Fig. 1(b), $C_{C,ij}$ describes the coupling capacitance between metal line segments *i* and *j*, and the approach in [15] was used to calculate such a capacitance. Coupling at the underpass was modeled using a parallel-plate capacitor.

3. MODEL VERIFICATION

A symmetrical, octagon inductor fabricated with the 0.35 μm CMOS technology was considered and measured to verify the model developed. The inductor was built on a 9.59 μm oxide and 500 μm silicon substrate. The inductor has 3 turns, metal width of 15 μm, metal thickness of 2 μm, and spacing of 8 μm. Two-port parameters were measured, and the inductance, resistance and quality factor of the inductor were extracted. In addition to the present model, two existing

inductor models developed intended for the asymmetrical inductors were considered and compared.

A systematic method to determine the values of the fitting parameters ($c1$ and $c2$) in (2) is needed. To this end, the following function was developed:

$$D = \sqrt{\sum_{l}\left(\frac{Q_{measure}(f_l) - Q_{model}(f_l)}{Q_{measure}(f_l)}\right)^2 + \sum_{l}\left(\frac{L_{measure}(f_l) - L_{model}(f_l)}{L_{measure}(f_l)}\right)^2} \quad (3)$$

where D describes the averaged error associated with fitting the model to the measured Q factor and inductance using different fitting parameter values at several different frequencies. The parameter value that yields the smallest D is the one to use, and $c1$ = 0.653 and $c2$= 0.53 were obtained from this approach for the spiral inductor considered.

Figs. 4(a)-(c) show the quality factor, inductance, and resistance, respectively, calculated from the present model, calculated from the two existing models, and obtained from measurements. The present model demonstrates a better accuracy over the existing models for a wide range of operating frequencies. Thus, our results suggested that it is erroneous and impractical to use the inductor model developed intended for asymmetrical inductors for predicting the characteristics of symmetrical inductors. The phase and magnitude of S_{21} parameter calculated from the models and obtained from measurements are compared in Figs. 4(d) and (e), respectively.

4. CONCLUSIONS

A compact and accurate model for spiral inductors has been developed. Unlike the existing models which were developed intended only for asymmetrical inductors, the present model was shown capable of predicting the characteristics of both the symmetrical and asymmetrical inductors accurately. Relevant device physics, such as the current crowding, overlap parasitics and geometry effect, have been taking into account.

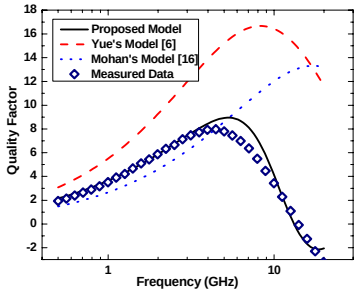

(a)

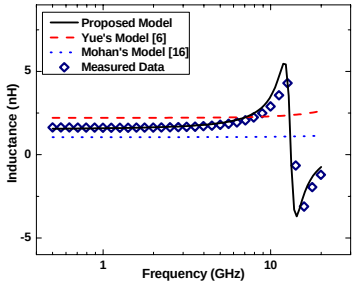

(b)

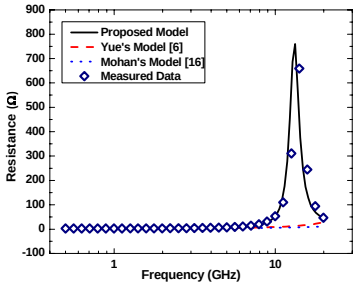

(c)

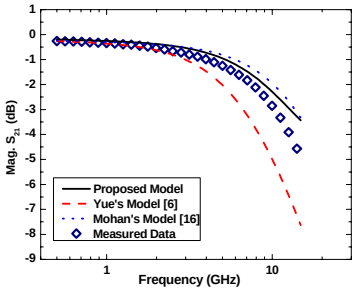

(d)

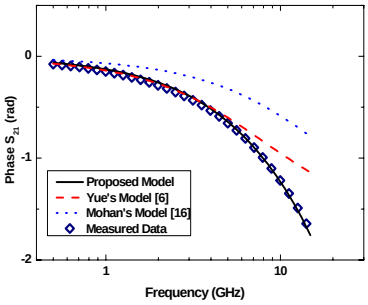

(e)

Fig. 4: Comparisons of the present model, existing models, and measurements of (a) quality factor (b) inductance, (c) series resistance, (d) S21 magnitude and (e) S21 phase for the 3-turn symmetrical inductor.

REFERENCES

[1] S. Chaki, S. Aono, N. Anodoh, Y. Sasaki, N. Tanino, and O. Ishihara, Digest of IEEE International Microwave Theory and Techniques Symposium, 1995.

[2] Mina Danesh and John R. Long, IEEE Trans. Microwave Theory and Techniques, vol. 50, Jan. 2002.

[3] Ban-Leong Ooi, Dao-Xian Xu, and Pang-Shyan Kooi, IEEE Radio Frequency Integrated Circuits Symposium, pages 259–262, June 2003.

[4] Sunderarajan S. Mohan, Doctoral dissertation, 1999.

[5] N. M. Nguyen and R. G. Meyer, IEEE Journal of Solid-State Circuits, vol. 25, pages 1028-1031, Aug. 1990.

[6] C. Patrick Yue and S. Simon Wong, IEEE Transactions on Electron Devices, vol. 47, March 2000.

[7] J. Crols, P. Kinget, J. Craninckx, and M. Steyeart, Digest of VLSI Circuits, pp. 28-29, 1996.

[8] J. Gil and H. Shin, International Conference on Simulation of Semiconductor Processes and Devices, pp. 35-38, Sept. 2003.

[9] Yu Cao, et al., IEEE Journal of Solid-State Circuits, VOL. 38, NO.3, March 2003

[10] A. Niknejad, http://rfic.eecs.berkeley.edu/~niknejad/ asitic.html

[11] Ansoft Corporation, HFSS, http://www.ansoft.com/products/hf/hfss/

[12] H. M. Greenhouse, IEEE Transactions on Parts, Hybrids, and Packaging, vol. 10, pages 101-109, 1974.

[13] Frederick W. Grover, "Inductance Calculations," New York, D. Van Nostrand Company, Inc. 1946.

[14] J. S. Yuan, W. R. Eisenstadt, and J. J. Liou, IEEE Trans. Components, Hybrids, and Manufacturing Technology, vol. 13, pp. 275-280, June 1990.

[15] G.L Matthaei,. G.C Chinn, C.H Plott, N Dagli, IEEE Transactions on Computer-Aided Design of Integrated Circuits and Systems, vol. 11, pp. 513-524, April 1992.

[16] Sunderarajan S. Mohan, Mari del Mar Hershenson, Stephen P. Boyd, and Thomas H. Lee, IEEE J. Solid-State Circuits, vol. 34, Oct. 1999.